Supporting Information for

Unraveling the Radiative Pathways of Hot Carriers upon Intense Photoexcitation of Lead Halide Perovskite Nanocrystals

Paris Papagiorgis[†], *Andreas Manoli*[†], *Sozos Michael*[†], *Caterina Bernasconi*[‡,#], *Maryna I. Bodnarchuk*[#], *Maksym V. Kovalenko*[‡,#], *Andreas Othonos*[‖] *and Grigorios Itskos*[†,*]

[†]Department of Physics, Experimental Condensed Matter Physics Laboratory, University of Cyprus, Nicosia 1678, Cyprus

[‡]Institute of Inorganic Chemistry, Department of Chemistry and Applied Biosciences, ETH Zürich, CH-8093 Zürich, Switzerland

[#]Laboratory for Thin Films and Photovoltaics, Empa – Swiss Federal Laboratories for Materials Science and Technology, Überlandstrasse 129, CH-8600 Dübendorf, Switzerland

[‖]Department of Physics, Laboratory of Ultrafast Science, University of Cyprus, Nicosia 1678, Cyprus

[*]itskos@ucy.ac.cy

Fit Parameters / Film type	Detection (eV)	Fluence <N>	$\frac{A_1}{A_1+A_2}$	τ_1 (ps)	$\frac{A_2}{A_1+A_2}$	τ_2 (ps)
Hot PL	**1.685**	8	0.52	19	0.48	770
Hot PL	**1.760**	8	0.62	15	0.38	808
Hot PL	**1.840**	8	0.77	10	0.23	789
Hot PL	**1.685**	16	0.46	16	0.54	895
Hot PL	**1.760**	16	0.57	12	0.43	903
Hot PL	**1.840**	16	0.70	8	0.30	989
ASE	**1.685**	8	0.64	20	0.36	440
ASE	**1.760**	8	0.92	16	0.08	402
ASE	**1.840**	8	1	8	-	-
ASE	**1.685**	16	0.60	18	0.40	525
ASE	**1.760**	16	0.86	14	0.14	595
ASE	**1.840**	16	1	8	-	-

Supplementary Table S1: Fitting parameters of the double-exponential model

$$-\frac{\Delta A}{A} = A_1 e^{-\frac{t}{\tau_1}} + A_2 e^{-\frac{t}{\tau_2}}$$

applied to fit the transient absorption curves of Suppl. Fig. 4, obtained at the bleaching region of hot PL/ASE $FAPbI_3$ NC films.

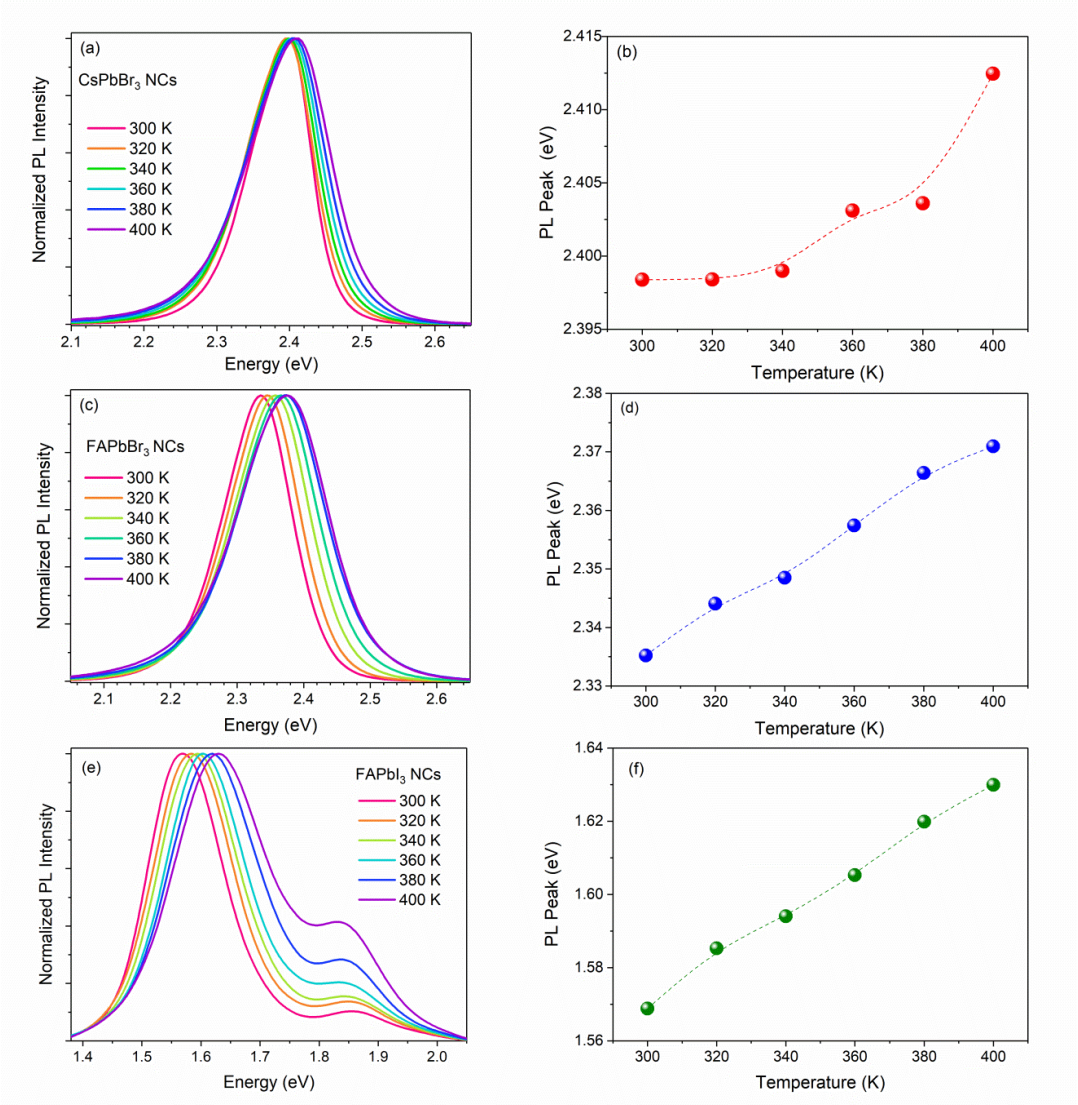

Supplementary Figure S1: Normalized PL spectra (left) and PL peak position (right) in the 300 K to 400 K temperature range from films of **(a), (b)** $CsPbBr_3$ NCs, **(c), (d)** $FAPbBr_3$ NCs, **(e), (f)** $FAPbI_3$ NCs.

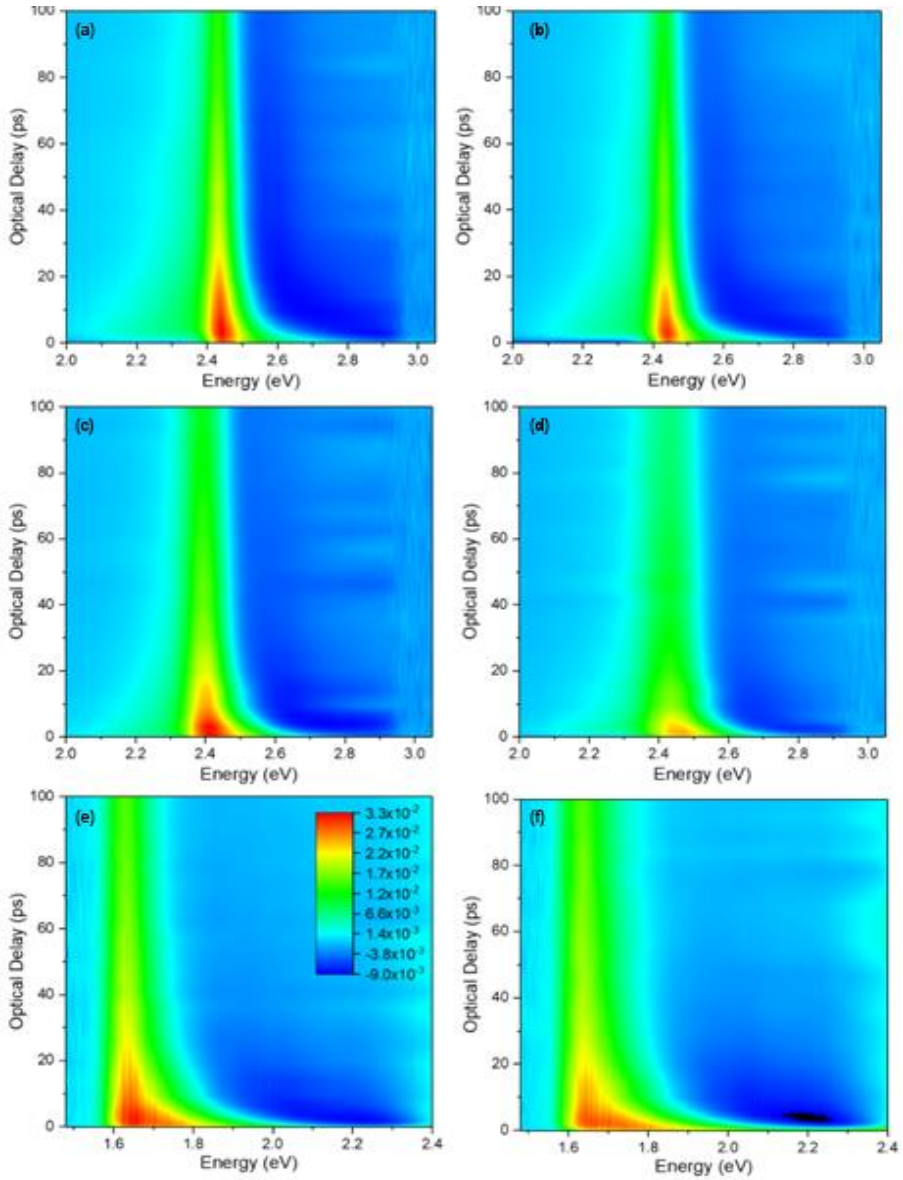

Supplementary Figure S2: Transient absorption (TA) contour plots in the 0 to 100 ps range for excitations of <N> ~8 (graphs on the left) and ~16 (graphs in the right) for a **(a), (b)** $CsPbBr_3$, **(c), (d)** $FAPbBr_3$ and **(e), (f)** $FAPbI_3$ NC film, respectively**.** The presence of long-lived hot carriers in all three NC materials is manifested by the high energy broadening of the bleaching TA signal that peaks around the energy gap of the three materials. The spectral width and lifetime of the high energy tail appears quite more pronounced in the $FAPbI_3$ NC film, which indicates a prolonged carrier cooling time in such solids.

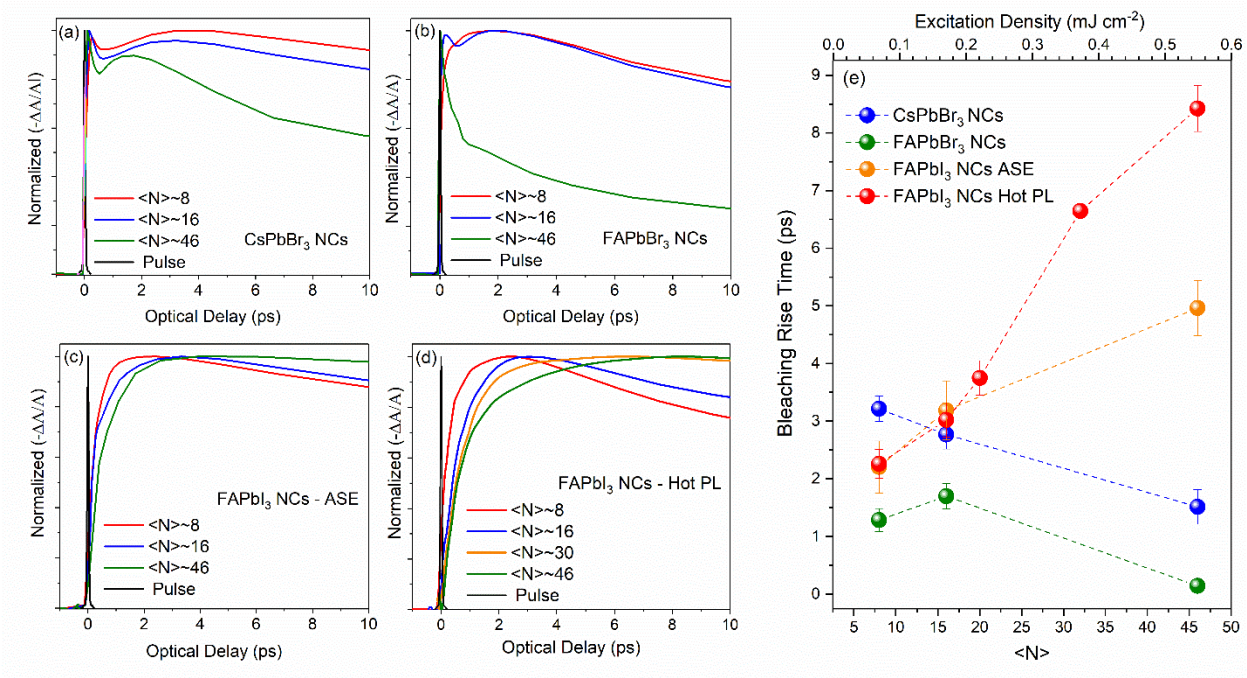

Supplementary Figure 3: Excitation-dependent TA early time dynamics at the bleaching region from **(a)** $CsPbBr_3$, **(b)** $FAPbBr_3$ and **(c)** $FAPbI_3$ NC - ASE and (d) $FAPbI_3$ NC – hot PL films. The pump excitation pulse is also displayed. (e) Dependence of the bleaching signal rise time to excitation fluence for the aforementioned films. The rise time provides a measure of the interband carrier relaxation time. The $FAPbI_3$ NCs films, show a monotonic excitation-dependent retardation of the build-up time, in contrary to the Br-containing NCs that assume an opposite trend, overall reducing with fluence. The effect may be interpreted by accounting the relatively long biexciton lifetimes reported for $FAPbI_3$ NCs [1,2] compared to the more efficient multiexciton relaxation observed in Cs-based NCs [3] and the activation of efficient Auger heating in the iodide-containing NCs [4]. On the other hand for the $FAPbI_3$ NC solids, hot PL films exhibit consistently slower bleaching rise times compared to those of the ASE films with the time difference increasing as higher fluences are employed i.e. at the highest excitation of <N> ~50 probed, the former exhibit a bleaching rise time more than two times slower than the respective signal in the latter films.

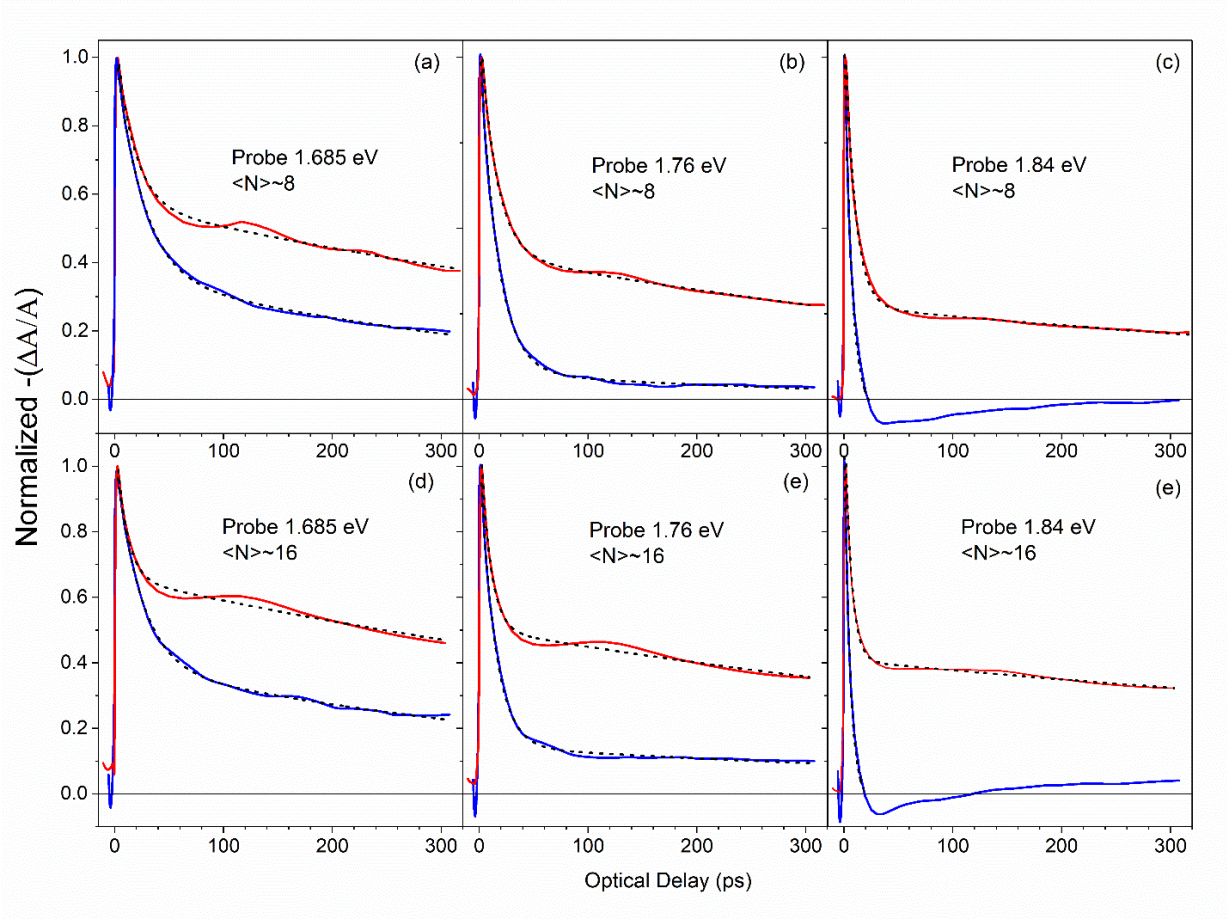

Supplementary Figure S4: Normalized TA transients fitted by a double-exponential model (dashed black line) from $FAPbI_3$ NC films exhibiting hot PL (red) and ASE (blue) for three probe wavelengths within the NC state filling region at photoexcitation of **(a), (b), (c)** <N> ~8 (~0.1 mJ cm^{-2}) and **(d), (e), (f)** <N> ~16 (~0.2 mJ cm^{-2}). faster TA dynamics to those of hot PL films. The extracted fitting parameters are presented **in Suppl. Table 1.**

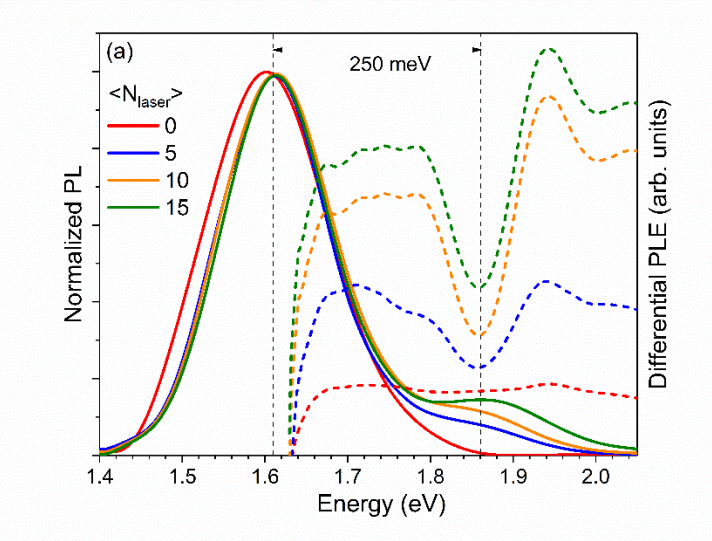

Supplementary Figure S5: Normalized, excitation-dependent PL spectra from a hot PL film, showing the emergence of new high energy emission peak at ~250 meV above the main NC PL. The origin of the unknown emission was explored in our work by employing a differential excitation PL (PLE) experiment in which the PLE signal monitoring the main PL peak, was excited by a monochromator-filtered Xe lamp beam in the presence and absence of a second beam from the second harmonic (532 nm) of an Nd:YAG laser. Details of the experiment are provided in the Materials and Methods. As seen in the graph, in the presence of the green laser beam, the differential PLE signal overall increases due to carrier filling of the NC states. However a pronounced and relatively narrow (FWHM ~80 meV) dip in the differential PLE signal, coincident with the spectral position of the new peak at the high excitation PL data, appears to evolve as the fluence of the 532 nm laser increases. The dip indicates a significant loss of the band-edge PL signal when the $FAPbI_3$ NCs are excited resonantly with the high energy PL peak, i.e. ~250 meV above the band gap. Based on such evidence, it appears that the new emission feature originates on a localized state that is not coupled to the manifold of the electronic states of the nanocrystals. As this emission feature appears more pronounced in material that has been exposed to intense

photoexcitation, high temperatures, repeated cooling and heating thermal cycles and UV photoexcitation, we tentatively assigned it to a localized defect state.

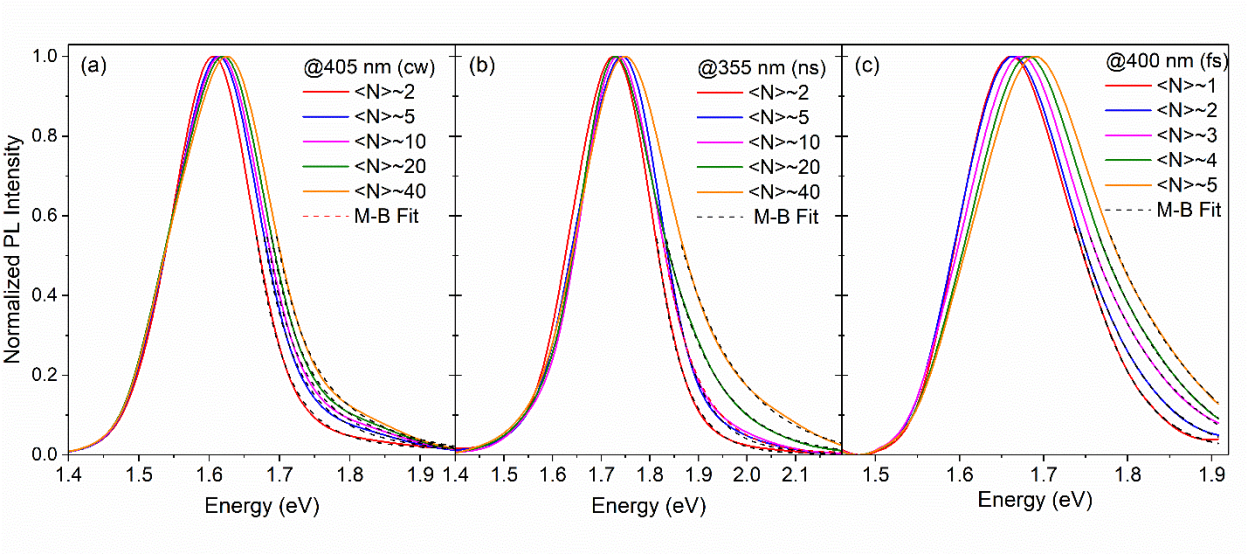

Supplementary Figure S6: Maxwell-Boltzmann curve fits of the high energy tail of excitation-dependent PL spectra from $FAPbI_3$ NC films excited by a **(a)** 405 nm continuous-wave, **(b)** 355 nm 5 ns pulsed and **(c)** 400 nm, 100 fs pulsed laser excitation.

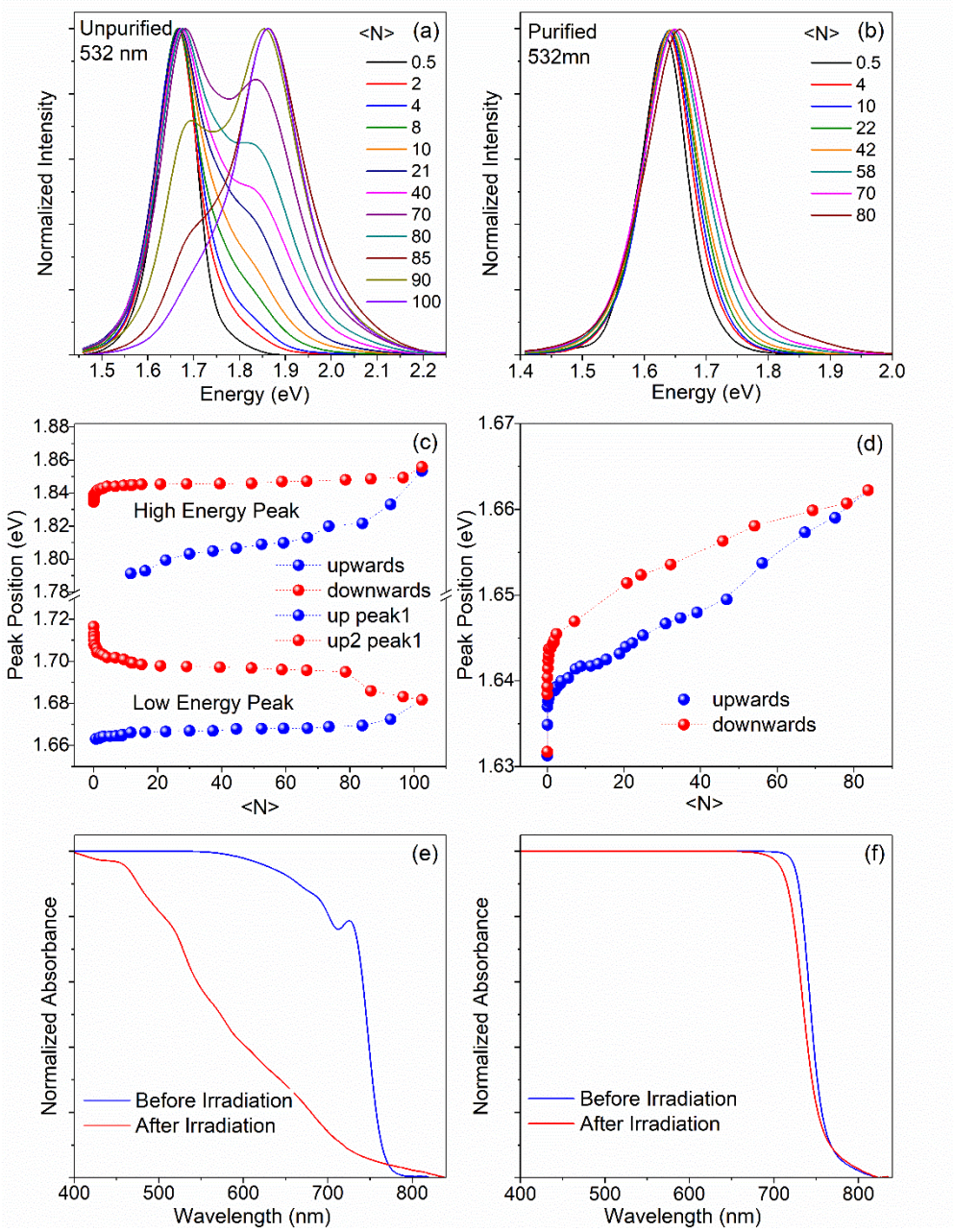

Supplementary Figure S7: Normalized photoluminescence spectra obtained at different excitation densities for 532 nm ns-excitation from **(a)** a non-purified $FAPbI_3$ NC solution and **(b)** a purified $FAPbI_3$ NC solution. Purified/Non-purified NC solution refers to material subjected/non-subjected to purification cycles by a non-solvent. Variation of the PL peak position with fluence under ramp up/down cycles for **(c)** the non-purified NC solution and **(d)** the purified

NC solution. Absorbance before (blue) and after (red) multiple irradiation cycles up to excitation energy densities of ~10 mJ cm^{-2} from **(e)** the non-purified and **(h)** the purified NC solutions. The data indicate that non-purified NC solutions exposed to intense UV or visible photoexcitation by nanosecond or femtosecond pulses exhibit typically an excitation-dependent quenching of the NC band-edge emission at the expense of the new emission feature discussed in the main text and assigned to a localized defect state. Furthermore, both of the two luminescence peaks assume a highly irreversible behavior upon ramp up/down processes of the excitation density while the integrity of the NCs is compromised as evidenced by the substantial irradiation-induced quenching of the optical absorption spectra. The aforementioned experimental evidence further supports the assignment of the high energy emission feature to NC defect radiative recombination. In contrary, luminescence in properly purified NC solutions is dominated by the NC ground state emission that exhibits a hysteretic but reversible excitation-dependent variation of the PL peak upon both green (532 nm) and UV (355 nm) photoexcitation and marginal variation of the absorbance lineshape upon multiple irradiation cycles up to high energy densities of ~9 mJ cm^{-2}.

References

1. Fang, H.-H.; Protesescu, L.; Balazs, D. M.; Adjokatse, S.; Kovalenko, M. V.; Loi, M. A. Exciton Recombination in Formamidinium Lead Triiodide: Nanocrystals Versus Thin Films, Small, 2017, 13, 1700673.

2. Eperson, G. E.; Jedlicka, E.; Ginger, D. S., Biexciton Auger Recombination Differs in Hybrid and Inorganic Halide Perovskite Quantum Dots, *J. Phys. Chem. Lett.* , **2018**, 9, 104−109.

3. Makarov, N. S.; Guo, S.; Isaienko, O.; Liu, W.; Robel, I.; Klimov, V. I., Spectral and Dynamical Properties of Single Excitons, Biexcitons and Trions in Cesium−Lead-Halide Perovskite Quantum Dots, *Nano Lett.*, **2016**, 16, 2349−2362.

4. Papagiorgis P.; Protesescu, L.; Kovalenko M. V.; Othonos, A.; Itskos, G., Long-Lived Hot Carriers in Formamidinium Lead Iodide Nanocrystals, *J. Phys. Chem. C* , **2017**, 121, 12434−12440.